Mechanism of Bloom syndrome complex assembly required for double Holliday junction dissolution and genome stability

Charlotte Hodson[a,1], Jason K. K. Low[b], Sylvie van Twest[a], Samuel E. Jones[c], Paolo Swuec[d,2], Vincent Murphy[a], Kaima Tsukada[c,e], Matthew Fawkes[c,f], Rohan Bythell-Douglas[a,g], Adelina Davies[d], Jessica K. Holien[g,h,i], Julienne J. O'Rourke[a], Benjamin L. Parker[b], Astrid Glaser[a], Michael W. Parker[i,j], Joel P. Mackay[b], Andrew N. Blackford[c,f], Alessandro Costa[d], and Andrew J. Deans[a,g,3]

[a]Genome Stability Unit, St. Vincent's Institute of Medical Research, Fitzroy, VIC 3065, Australia; [b]School of Life and Environmental Sciences, University of Sydney, Sydney, NSW 2006, Australia; [c]Department of Oncology, MRC Weatherall Institute of Molecular Medicine, University of Oxford, John Radcliffe Hospital, Oxford OX3 9DS, United Kingdom; [d]Francis Crick Institute, London NW1 1AT, United Kingdom; [e]Laboratory for Zero-Carbon Energy, Institute of Innovative Research, Tokyo Institute of Technology, Tokyo 152-8550, Japan; [f]MRC Oxford Institute for Radiation Oncology, Department of Oncology, University of Oxford, Oxford OX3 7DQ, United Kingdom; [g]Department of Medicine (St. Vincent's), University of Melbourne, Fitzroy, VIC 3065, Australia; [h]School of Science, RMIT University, Melbourne, VIC 3001, Australia; [i]Structural Biology Unit, St. Vincent's Institute of Medical Research, Fitzroy, VIC 3065, Australia; and [j]Bio21 Institute, University of Melbourne, Parkville, VIC 3010, Australia

The RecQ-like helicase BLM cooperates with topoisomerase IIIα, RMI1, and RMI2 in a heterotetrameric complex (the "Bloom syndrome complex") for dissolution of double Holliday junctions, key intermediates in homologous recombination. Mutations in any component of the Bloom syndrome complex can cause genome instability and a highly cancer-prone disorder called Bloom syndrome. Some heterozygous carriers are also predisposed to breast cancer. To understand how the activities of BLM helicase and topoisomerase IIIα are coupled, we purified the active four-subunit complex. Chemical cross-linking and mass spectrometry revealed a unique architecture that links the helicase and topoisomerase domains. Using biochemical experiments, we demonstrated dimerization mediated by the N terminus of BLM with a 2:2:2:2 stoichiometry within the Bloom syndrome complex. We identified mutations that independently abrogate dimerization or association of BLM with RMI1, and we show that both are dysfunctional for dissolution using in vitro assays and cause genome instability and synthetic lethal interactions with GEN1/MUS81 in cells. Truncated BLM can also inhibit the activity of full-length BLM in mixed dimers, suggesting a putative mechanism of dominant-negative action in carriers of BLM truncation alleles. Our results identify critical molecular determinants of Bloom syndrome complex assembly required for double Holliday junction dissolution and maintenance of genome stability.

Bloom's complex | topoisomerase | cross-link mass spectrometry | helicase | genome stability

Homologous recombination (HR) is an essential and highly regulated cellular process required for maintenance of genome stability during mitosis and sexual reproduction. A key intermediate in HR and recombinational DNA repair is a four-way DNA junction known as a Holliday junction (HJ). During meiosis, double Holliday junctions (dHJs) are cut by endonucleases (resolution) in order to create the cross-overs necessary for proper chromosome segregation (1, 2). In somatic cells, however, cross-overs are potentially deleterious, and their formation is suppressed by the BLM protein (3). Failure to suppress cross-over formation leads to an increased frequency of sister chromatid exchanges and has the potential to result in translocations and/or somatic cell loss of heterozygosity (4), key drivers of genome instability and cancer. As a likely consequence, individuals with homozygous *BLM* mutations exhibit Bloom syndrome and are highly cancer prone (5). Heterozygous *BLM* mutation carriers are also significantly overrepresented in breast cancer families (6, 7).

The 1,417-amino acid BLM protein suppresses DNA cross-overs by promoting dHJ "dissolution," a process that unlinks the recombination intermediates back to their prerecombination state (8). Critical to dHJ dissolution by BLM is a RecQ-type superfamily II helicase domain. The ATPase function of this domain is required for DNA unwinding, translocation, and strand exchange within the HJ (9, 10). Dissolution also requires the concerted action of three additional factors, topoisomerase IIIα (TopoIIIα), RMI1, and RMI2. Together, these four proteins form the Bloom syndrome complex (BS complex; also

Significance

Bloom syndrome complex (BS complex) is necessary for maintenance of genome stability and suppression of cancer-causing mutations. Composed of a helicase, a topoisomerase, and two scaffolds, the BS complex is implicated in several steps that ensure the high fidelity of DNA repair by recombination. One step, called "double Holliday junction dissolution," ensures untangling of DNA at the conclusion of repair. Here, we used cross-link mass spectrometry to show how the BS complex assembles. Using biochemical reactions and cell complementation with mutant proteins, our results reveal an important role of helicase dimerization (and tight coupling of proteins within the complex) for double Holliday junction dissolution and genome stability.

BIOCHEMISTRY

known as the "dissolvasome" or "BTRR [BLM-TopoIIIα-RMI1-RMI2]") (11). TopoIIIα belongs to the type IA class of topoisomerases, padlock-shaped enzymes that effect changes in DNA topology through a "strand-passage" mechanism (12). When coupled with TopoIIIα, BLM promotes DNA decatenation under physiological conditions by catalyzing DNA unlinking in an ATPase-dependent manner.

The ancillary factors RMI1 (625 amino acids) and RMI2 (147 amino acids) are Replication Protein A–like, OB (oligonucleotide binding) fold–containing proteins that stimulate the dissolution reaction and have been implicated in either nucleic acid engagement (13–15) or protein–protein interactions (16–19). In particular, in the yeast dissolvasome complex, RMI1 stabilizes the covalently bound open form of the TopoIIIα DNA gate in a configuration that favors DNA strand passage (10). The significance of these components to BLM function is underscored by recent discoveries of homozygous mutant *TOP3A*, *RMI1*, or *RMI2* individuals who have Bloom syndrome–like disorders (20, 21).

X-ray crystal structures of the RecQ helicase domain of BLM [encompassing residues 636 to 1298, Protein Data Bank (PDB) ID codes 4CGZ, 4CDG, and 4O3M (22, 23)] revealed a unique position of the DNA duplex relative to the helicase core and visualization of both pre- and posttranslocation states that flip out at least three bases of single-strand DNA (ssDNA). An additional structure of TopoIIIα (residues 21 to 639) in complex with RMI1 [residues 2 to 216; PDB ID code 4CHT (12)] also revealed the characteristic toroidal structure of type I topoisomerases, with a gate mechanism that is regulated by an insertion loop within the first OB fold of RMI1. While these structures informed on key residues and the biophysical action of each protein, they did not explain how the BS complex assembles or point to an overall mechanism of dHJ dissolution. Key to understanding this mechanism is a molecular characterization of the number and relative position of helicases and topoisomerases within the complex. However, there are contrasting reports in the literature on the oligomeric state of BLM. Size exclusion chromatography and atomic force microscopy support monomeric, dimeric, and larger oligomeric states, while EM data reveal five- or six-lobed structures reminiscent of ring-shaped multimeric ATPases (24–27). The oligomeric state of BLM within the BS complex has never been investigated, although RMI1:RMI2 purified in isolation forms a 1:1 heterodimer in published reports (16, 18, 19).

The primary goal of this study was to establish how the BS complex assembles and how this assembly promotes dHJ dissolution and maintenance of genome stability. To achieve this, we purified an active recombinant BS complex. Using a combination of biochemical, biophysical, and cross-linking mass spectrometry (XL-MS) experiments, we determined that recombinant BS complex exists predominantly in a 2:2:2:2 stoichiometry. We found that dimerization of the BS complex and interaction with TopoIIIα/RMI1 are mediated by the N terminus of BLM, and we define critical residues required for these interactions and dHJ dissolution in vitro. To validate our in vitro experiments, we used cell complementation experiments with mutant BLM proteins and showed that these interactions are also required for genome stability in cells.

Results

Purification of the Active Recombinant BS Complex. To investigate the molecular assembly of the BS complex, we used the Multibac expression system (28) to purify the recombinant complex containing BLM-His, TopoIIIα, maltose binding protein (MBP)-RMI1, and RMI2. Coexpression of the four proteins in baculovirus-infected insect cells resulted in the formation of a salt-stable stoichiometric complex (Fig. 1 *A* and *B*). We
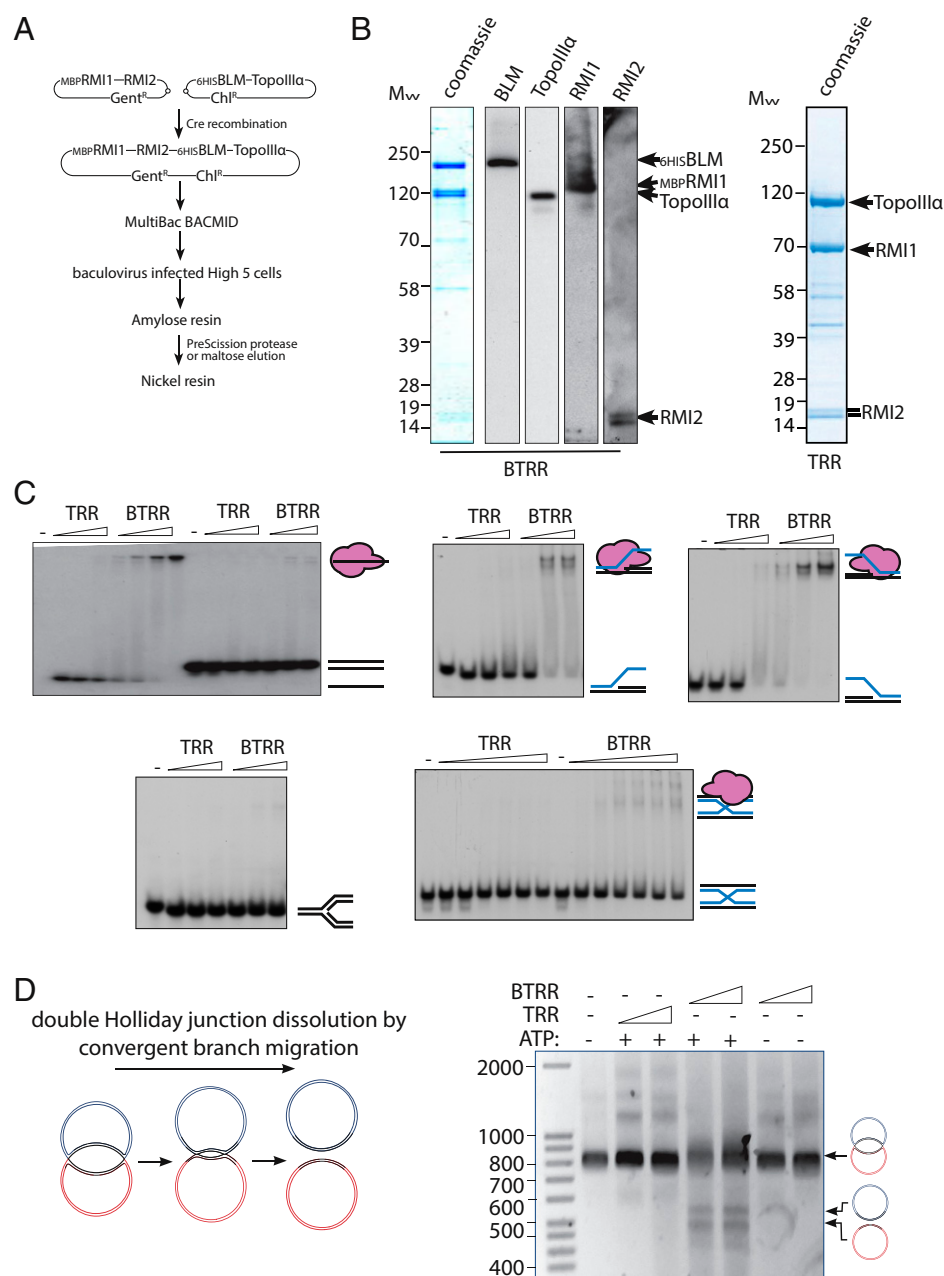
also found that TopoIIIα, MBP-RMI1, and RMI2 form a similarly stable stoichiometric complex without BLM being present (Fig. 1*B*).

In isolation, BLM, TopoIIIα, and RMI1 are known to bind DNA (15, 29, 30). To determine the DNA binding properties of the intact BS complex, we performed electromobility shift assay (EMSA) experiments using oligonucleotide-based replication and recombination intermediates (Fig. 1*C*). We found that the BS complex has DNA binding specificity for ssDNA, 5′- and 3′-flap structures, and lower affinity for four-way immobile HJ and replication fork structures, while the complex lacking BLM (TRR) displays a weaker affinity for the same structures (Fig. 1*C*). Using EMSA, neither complex demonstrated stable interaction with double-stranded DNA that lacks secondary structure. These findings are consistent with a large body of evidence indicating that the BS complex is specifically active in vivo on DNA sequences containing ssDNA and branch point structures.

Although we showed that the BS complex has lower affinity for HJ structures compared with 5′ and 3′ flap–containing sequences, the sequences within oligonucleotide mimics are immobile. In contrast within a dHJ structure, the junction point of a four-way junction can be moved by translocation because of the homologous nature of sequences residing at either side of the branch point. This DNA arrangement is present within a more complex plasmid-based "ideal dHJ" structure, originally created by Plank and Hsieh (31). This covalently closed ideal dHJ contains junctions on either side of a 165-bp sequence of homology and has a linking number of ∼30 (31). We found that the recombinant copurified BS complex promoted ATP-dependent dHJ dissolution of the ideal dHJ, leading to the formation of two closed circular DNA products (Fig. 1*D*). In contrast, the TopoIIIα-RMI1-RMI2 complex lacking BLM was deficient in this activity (Fig. 1*D*). These results demonstrate that the intact copurified BS complex is active on dHJ substrates normally found during HR.

Protein Cross-Linking Reveals Subunit Organization within the BS Complex. Despite the tantalizing evidence that BLM and TopoIIIα act together to directly couple a helicase and topoisomerase activity, how they interact is not well understood, and in no instances have mutants been identified that could uncouple their activity. To inform the mechanism of the BS complex assembly, we utilized XL-MS. XL-MS analyses can provide positional information on flexible, transient, and modular higher-order multiprotein complexes by mapping regions of spatial proximity. In our experiments, we used disuccinimidyl suberate (DSS) to specifically cross-link primary amines (i.e., lysine residues and protein N termini) (32). An example of a cross-linked sample of the MBP-BTRR complex is shown in Fig. 2*A*. Trypsin-digested products enriched for cross-linked peptides were analyzed by mass spectrometry (LC-MS/MS) to identify the cross-linked peptides (Fig. 2*B*).

A total of 170 cross-links were identified using the analysis software xQuest and pLINK (33, 34) across three experiments, with 65 identified in at least two replicate experiments; 153 were determined to be intraprotein cross-links, and 17 were interprotein cross-links (Dataset S1). We mapped all 170 cross-links on a two-dimensional schematic of the complex (Fig. 2*D*). No cross-links were observed for RMI2; this is probably due to it being a small protein (16 kDa) with only three lysine residues. Interestingly, very few cross-links were observed in the N-terminal half of BLM and the N-terminal half of RMI1 (Fig. 2*D*). These regions are not lysine "deserts." Instead, the identification of a large number of monolinks (one-ended reactions with the cross-linker) or short intrapeptide cross-links (cross-links within a single tryptic peptide, loop links) reveals that both RMI2 and the N terminus of BLM and RMI1 were accessible to cross-linking agents (*SI Appendix*, Fig. S1). However, the structural arrangement of these parts of the protein do not

2 of 12 | PNAS
https://doi.org/10.1073/pnas.2109093119

Hodson et al.
Mechanism of Bloom syndrome complex assembly required for double Holliday junction dissolution and genome stability

Fig. 1. Purification of stoichiometric, stable, and active recombinant BS complex. (*A* and *B*) Purification strategy and Coomassie blue–stained SDS-PAGE (sodium dodecyl sulfate-polyacrylamide gel electrophoresis) gels of the recombinant BS complex, including western blots for indicated proteins. (*C*) DNA binding EMSAs of the BS complex (BTRR) vs. complex-lacking BLM (TRR). EMSAs were performed with different oligonucleotide DNA structures depicted by the schematic next to the corresponding autoradiograph. (*D*) Schematic of the dHJ dissolution assay and products of convergent branch migration by recombinant Bloom complex (BTRR) and complex lacking BLM (TRR) in the presence or absence of ATP.

place lysines within the required proximity for interpeptide cross-linking.

Of the 170 cross-links, a total of 51 (48 intra and 3 inter) had both linked residues present in the available crystal structures (PDB ID codes 4CGZ, 4CDG, and 403M for BLM and 4CHT for TopoIIIα-RMI1). Additionally, we modeled in two loop regions 1,092 to 1,107 and 1,194 to 1,206 of the BLM structure using the SYBYL-X software suite. The maximal length of the DSS spacer that links two amine groups together is 11.4 Å. Based on previous published studies of validated XL-MS analyses (35), we used a maximal cutoff of 32 Å between C-α when comparing our data with available crystallographic data. This value incorporates 21 Å for lysine side chains (6 to 6.5 Å each)

and 4-Å "buffers" to partially account for protein dynamics. The online server xwalk was used to calculate Euclidean lengths of cross-linked pairs (36).

Overall, 81% (41 of 51) of cross-links fit within our cutoff of 32 Å, with 93% (38 of 41) of them being <28.5 Å. This distribution is similar to other published XL-MS datasets (see Fig. 4C) (32, 37). A total of 10 intraprotein cross-links fall above the maximal cutoff of 32.4 Å, 5 in each of TopoIIIα and BLM. For BLM, one of these cross-links is just above the cutoff measuring at 33.3 Å; the other four will be discussed in detail below. The cross-links that do not fit the current crystal structure of TopoIIIα all involve contacts between type 1A topoisomerase domains I and IV, which are proposed to undergo large
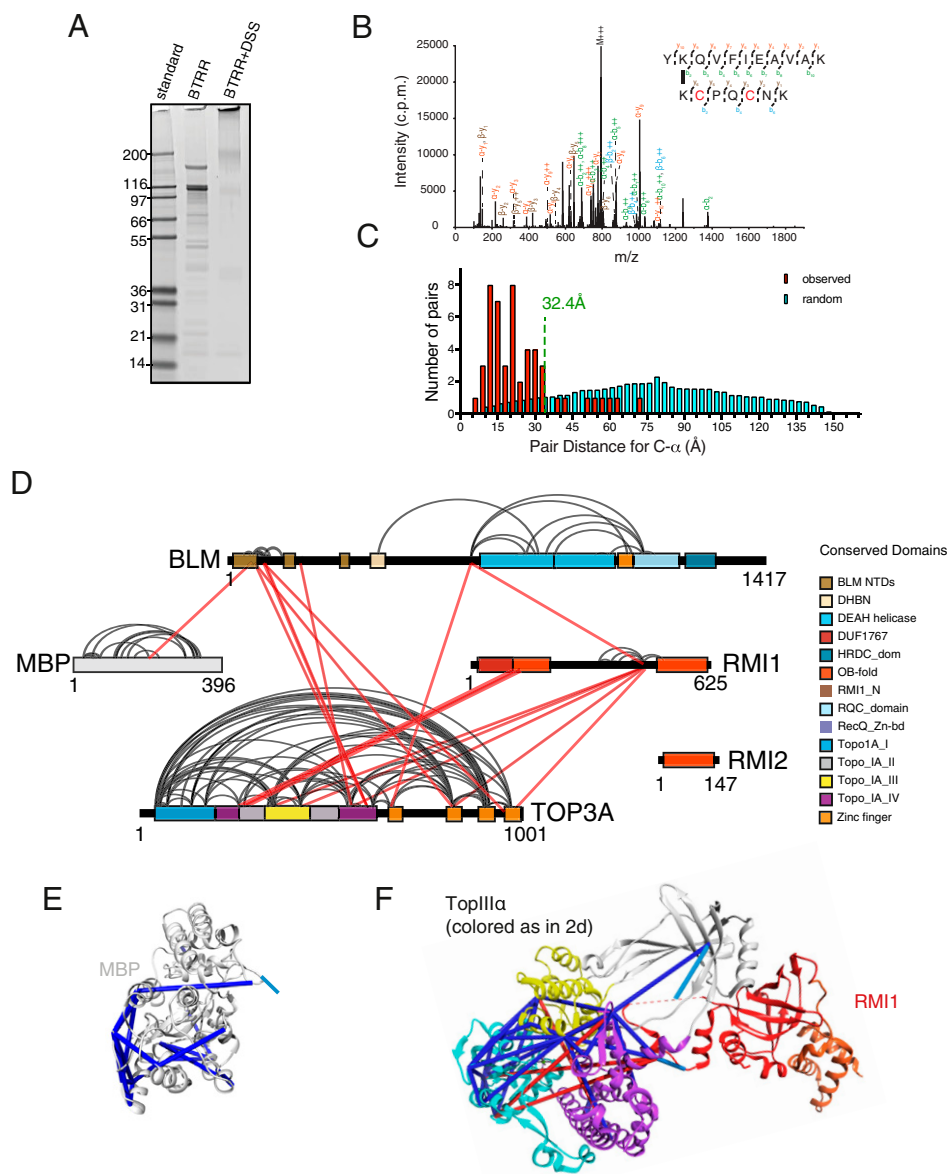
Fig. 2. Contact points within the BS complex revealed by cross-linking coupled mass spectrometry. (*A*) Sypro Ruby–stained gel of the BS complex before cross-linking with DSS (lane 2) and after treatment (lane 3). (*B*) Example of cross-link data and (*C*) distribution of the lengths of cross-linked peptides when mapped onto available crystal structures. (*D*) Schematic of the BS complex with mapped cross-linked peptides. Black lines represent intracross-links. Intercross-links are represented by red lines. (*E* and *F*) Example mapping of cross-links onto MBP (PDB ID code 1MPD) and TopoIIIα:RMI1 (PDB ID code 4CHT) crystal structures. Blue and red lines represent cross-links <33.4- and >33.4-Å cutoff, respectively. NTDs, amino terminal domains; c.p.m., counts per mass; m/z, mass/charge.

conformational changes between the open and closed states (38). Therefore, a possible explanation as to why these cross-links do not fit the current crystal structure is that the protein might exhibit considerable flexibility in solution.

An important control for our experiments concerned the identification of intraprotein cross-links within the MBP affinity tag on the RMI1 protein. MBP forms two compact globular domains (39). In our experiments with the recombinant MBP-tagged BS complex, we detected 19 intracross-links for MBP. All 19 fit the crystal structure (PDB ID code 5E7U) within the 32.4-Å limit (Fig. 2*E*). A further 17 loop links and 27 monolinks map to surface-accessible residues of MBP (*SI Appendix*, Fig. S1). Overall, the large percentage of cross-links falling within the maximum distance limits for the DSS cross-linker and the absence of unsupported intraprotein or interprotein cross-links within MBP provide confidence in the XL-MS data.

In addition to cross-links that can be cross-referenced to the partial crystal structures of the BS complex components, we were also able to identify structural information. For example, cross-linking is observed between the four zinc fingers of Top-oIIIα, suggesting that the C-terminal region of TopoIIIα is

globular and compact (Fig. 2*D*). Furthermore, zinc fingers 2 and 3 show multiple cross-links with the TopoIA DNA gate domain. This observation fits with the previous suggestion that the zinc fingers are involved in DNA binding and regulation of TopoIIIα activity (40). RMI1 residues 109 and 125 also cross-link with the TopoIA gate region of TopoIIIα, corresponding to the previously described contact in the loop region of RMI1 that regulates opening and closing of the Top1A gate (12) (Fig. 2*F*). Interprotein cross-links between the N terminus of BLM contact the rest of the complex via the C-terminal regions of both RMI1 and TopoIIIα. The majority of these map to the first 200 amino acids of BLM, consistent with previous yeast two-hybrid and truncation pull-down experiments (41).

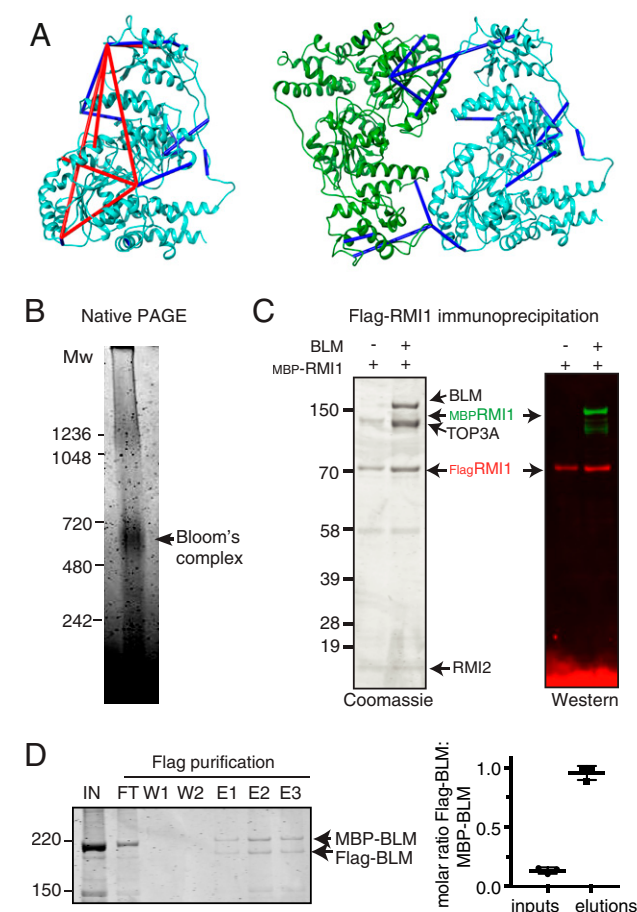**BLM Homodimerization Can Explain Unresolved Cross-Links within the BS Complex.** The existence of several intraprotein cross-links in BLM that deviate substantially from the known crystal structure (PDB ID code 4O3M, residues 640 to 1,298) can be rationalized by several explanations. First, the RecA fold of the BLM protein might undergo substantial reconfiguration when it forms the BS complex. This is unlikely because the presence

of other cross-links supports the retention of the overall fold of this functional domain (Fig. 2D and discussed above). Second, the cross-links might be assigned incorrectly. This is also unlikely given the high confidence of these hits relative to other well-supported cross-links. Third, these supposedly intraprotein cross-links might instead be interprotein cross-links that capture interactions between two different BLM molecules within the complex. Consistent with this hypothesis, previous studies have pointed to oligomerization with the BS complex (reviewed in ref. 11). Similar data supported the conclusion that FANCB-mediated dimerization of the Fanconi anemia core complex (42) was later supported by high-resolution cryo-EM (43).

To corroborate this idea, we used homology modeling and computational protein–protein docking to create a BLM homodimer assembly that is restrained by the deviating intraprotein

Fig. 3. BLM is a dimer within the Bloom complex and in isolation. (*A*) Cross-links mapped onto a monomer (*Left*) or dimer (*Right*) of BLM (PDB ID code 4O3M). Blue and red lines represent cross-links <33.4- and >33.4-Å cutoff, respectively. (*B*) The native PAGE gel shows a predominant band of greater than 500 kDa corresponding to the intact Bloom complex larger than its predicted molecular mass. (*C*) Copurification of MBP-BLM containing the Bloom complex shows that additional copies of Flag-BLM are present in maltose elutions. Coomassie-stained SDS-PAGE with components of the HJ dissolvasome is indicated. (*D*) Copurification of MBP-BLM and Flag-BLM in the absence of other Bloom complex components. IN is the input product of amylose purification, where the molar-normalized (1.25× factor based on the size difference between two proteins) Coomassie blue–stained MBP-Blm and Flag-BLM are indicated. After a second affinity purification on anti-Flag resin, the ratio between MBP-BLM and Flag-BLM is now approximately one. Error bars and values from three independent replicates of this experiments are shown. E1/2/3, Flag elutions; FT, flow through; W1/2, washes.

cross-links. The best model was then minimized using molecular dynamics, giving a final complex energy of –317,211.72 kcal/mol. The interface itself contained five hydrogen bonds, two salt bridges, and an interface area of 1,084.7 Å. Furthermore, according to protein interfaces, surfaces and assemblies service (PISA) at European Bioinformatics Institute, there was a 4.0-kcal/mol benefit of the two monomers interacting, and the solvation free energy *P* value of 0.5 suggests that the interface is not surprising. The resultant model showed that the violated intraprotein cross-link lengths of 66.5, 36.3, 50.1, and 33.0 Å were resolved to nondeviating interprotein cross-links of 17.8, 26.1, 30.2, and 32.1 Å, respectively (Fig. 3A). A fifth cross-link Lys1009 to Lys787 measured 53.3 Å in a monomeric BLM and 32.6 Å in the dimer model, which is just outside our cutoff of 32 Å. Further, we found that a significant number of the BLM-BLM cross-links that were satisfied in the monomeric structure also fit within the cutoff length for their placement as "interprotein" cross-links between two different BLM molecules. Finally, we found through structure-based alignment that our cross-link–derived BLM dimer model places the two RecQ helicase motifs into the same relative orientation as those found in RECQ1 dimer. RECQ1 is a human paralog of BLM, which forms dimers that are also required for branch migration of HJs (44). BLM dimer and RECQ1 dimer differ over 634 amino acids of the core RecQ folds by an rmsd of 2.292 Å (*SI Appendix*, Fig. S2 *A*–*C*). These findings strongly support the notion that BLM forms a higher-order assembly within the BS complex.

Dimerization of the BS Complex Is Mediated by the N Terminus of BLM. To identify whether and how a dimer may assemble, we undertook experiments to establish the stoichiometry of the BS complex. Although size exclusion chromatography of the complex was inconclusive, the BLM complex predominantly migrated on blue native polyacrylamide gel electrophoresis (PAGE) to a position between the 480- and 720-kDa markers (Fig. 3B). This is considerably larger than the predicted size of a complex containing one subunit of each protein (355 kDa). Because there is previous evidence that BLM forms dimers or multimers (24–27), we sought to determine whether BLM might induce an increase in the stoichiometry of other subunits in the BS complex. To do this, we carried out coexpression and purification of two TopoIIIα-RMI1-RMI2 complexes, one with MBP-tagged RMI1 and the other with Flag-tagged RMI1. When this was performed in the absence of BLM, the two tagged forms of RMI1 are not copurified, suggesting that TopoIIIα-RMI1-RMI2 forms only a heterotrimer (Fig. 3C). However, when BLM was also coexpressed, it is possible to observe multiple copies of TopoIIIα-RMI1-RMI2 in the BS complex (Fig. 3C). This finding suggests that BLM brings together the two differently tagged copies of the other subunits within the BS complex.

To determine the oligomeric state of BLM itself, we next performed a similar set of experiments in the absence of TopoIIIα-RMI1-RMI2. We used two-step affinity purification from extracts in which differently tagged forms of BLM were expressed. In the first purification step, MBP-BLM copurified a small amount of Flag-BLM. A subsequent Flag affinity purification led to the elution of MBP-BLM and Flag-BLM in a 1:1 stoichiometry (Fig. 3D). This strongly suggests that BLM is predominantly dimeric when purified in isolation and potentially dimeric within the BS complex.

Together, these results suggest the BS complex comprises two each of BLM, TopoIIIα, RMI1, and RMI2.

The DHBN Domain of BLM Mediates Dimerization of the BS Complex. BLM helicase is a large enzyme that contains multiple regions of conservation in its N-terminal half in addition to a very highly conserved C-terminal half containing the RECQ helicase

BIOCHEMISTRY
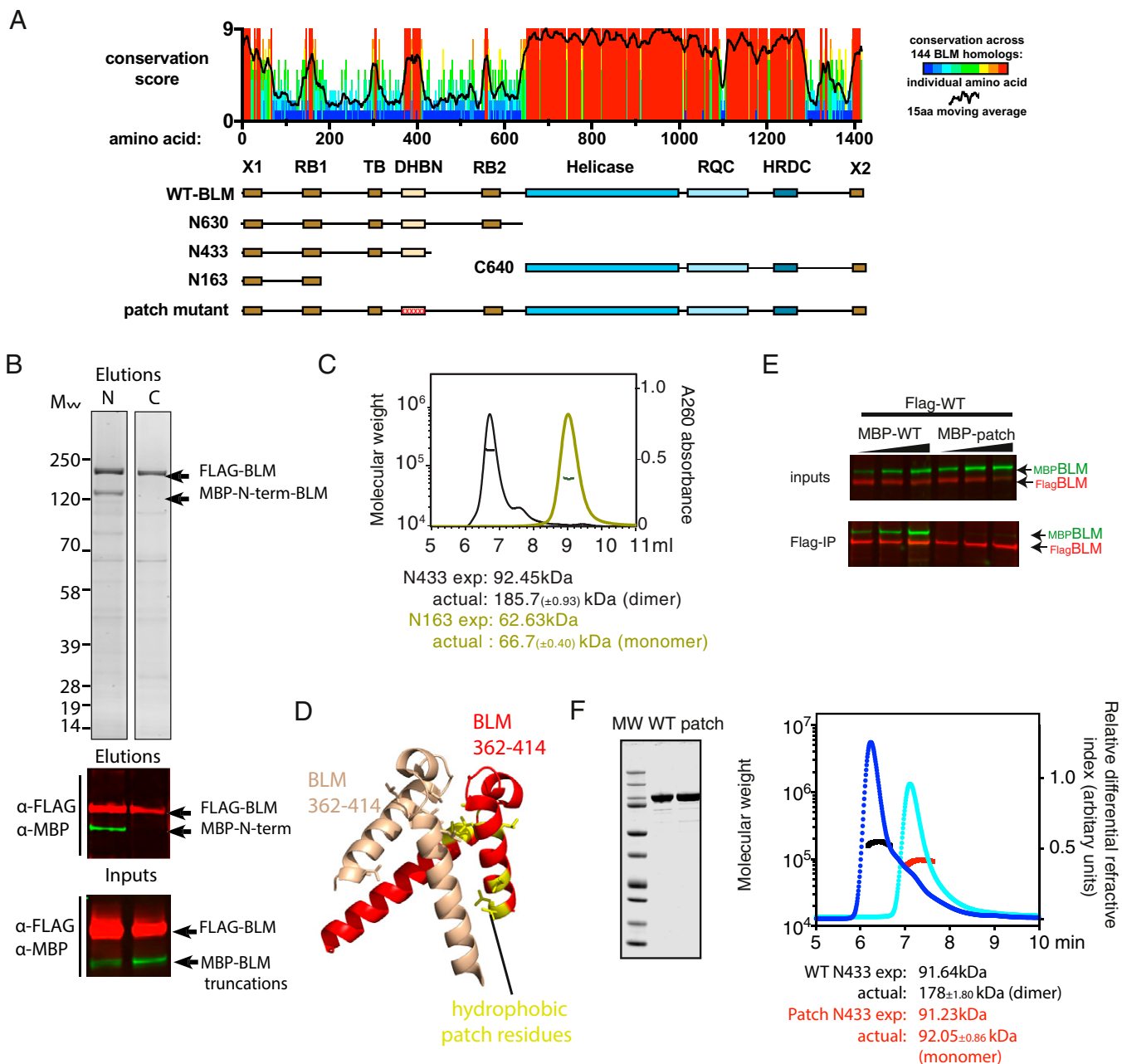
Fig. 4. The N-terminal DHBN domain mediates BLM dimerization. (*A*) Schematic of evolutionary conservation of the BLM helicase (144 vertebrate homologs) shown aligned to human BLM and known domains. Truncations used in this manuscript are shown below. DHBN, dimerization helical bundle in N terminus; HRDC, helicase and RNaseD C terminus; RB, RPA binding region 1 or 2; RQC, RecQ C terminus; TB, TOPBP1 binding region; X1/2, conserved motifs of unknown function. (*B*) Pull downs of MBP-tagged BLM-N630 or BLM-C640 with Flag-BLM. *Top* is Coomassie blue–stained SDS-PAGE gels. *Middle* and *Bottom* are anti-Flag (red) and anti-MBP (green) western blots of the elutions and inputs. Note that BLM-N630 and BLM-C640 fragments run at the same size by western blot. (*C*) SEC-MALS of BLM N-terminal fragments; overlayed are the profiles of BLM N1433 (black), and BLM N163 (yellow). (*D*) The crystal structure of the DHBN domain of BLM (PDB ID code 5LUP) showing that two BLM molecules (red and beige) form a dimerization interface. Side chains at the interface are depicted in yellow and shown by sequence alignment to be conserved in evolution. (*E*) The indicated "patch mutant" in *C* when cloned into full-length MBP-BLM does not coprecipitate with Flag-BLM. (*F*) The BLM N433 PATCH mutant is monomeric by SEC-MALS. WT, wild type.

core (Fig. 4*A*). To determine how BLM assembles a dimeric BS complex, we expressed N- or C-terminal fragments (N630 = residues 1 to 630 or C640 = 640 to ,1417, respectively). Even though we had observed cross-links between C-terminal parts of BLM in our XL-MS experiments (Figs. 2 and 3), coexpression studies showed that only the N-terminal half of the protein was able to stably copurify with the full-length Flag-BLM protein. This confirms previous reports that an N-terminal part of BLM can drive oligomerization (Fig. 4*B*) (11) and suggests that N-terminal

dimerization drives the colocalization of two C-terminal helicase domains within the intact BS complex.

To identify the dimerization interface within BLM, we designed two C-terminal truncations within the amino-terminal half of the protein, encompassing residues 1 to 163 (N163) or 1 to 433 (N433). According to size exclusion–coupled multiangle light scattering (SEC-MALS) measurements (Fig. 4*C*), MBP-BLM$_{N433}$ dimerizes (absolute molecular mass of 185.7 ± 0.9 kDa), whereas MBP-BLM$_{N163}$ is a monomer (66.7 ± 0.4 kDa),

in good agreement with its predicted monomeric mass of 62.63 kDa. These data narrow the dimerization interface to residues 164 to 433.

We note that this region of BLM contains the recently described DHBN domain (residues 362 to 414), a highly conserved domain that forms a dimeric packing interface in an X-ray crystal structure of this region (45). Within the DHBN, a patch of hydrophobic residues mediates the interface between the dimer pairs (Fig. 4D). We mutated this hydrophobic patch in full-length BLM to create MBP-BLM[PATCH]. We observed that MBP-BLM[PATCH] no longer copurifies with full-length wild-type Flag-BLM in pull-down experiments, despite being expressed at similar levels (Fig. 4E). Furthermore, an MBP-BLM N433[PATCH] mutant is monomeric by SEC-MALS (Fig. 4F) and does not change state when the MBP tag is removed (*SI Appendix*, Fig. S3A). These results confirm that the N-terminal DHBN domain mediates dimerization of the full-length BLM protein.

The N Terminus of BLM Mediates Interaction with TRR Independent of Its Dimerization. To determine which part of BLM mediates the association with the TopoIIIα:RMI1:RMI2 subunits, we assessed the BLM N630 or C640 fragments for interaction with TRR by coexpression and pull-down experiments (Fig. 5A). We found that in addition to the homodimerization domain, the N terminus is

also responsible for driving the main interaction with TRR. Nonetheless, interaction with TRR is independent of dimerization because TRR can still copurify with MBP-BLM[PATCH] (Fig. 5B).

Because multiple lines of evidence point to a direct interaction between BLM N163 and RMI1 being central to the formation of the BS complex, we worked to further define this interaction. We synthesized a 20–amino acid overlapping peptide array covering the BLM N163 fragment. On this membrane, each peptide overlapped the next by 19 amino acids, leading to a change of just 1 amino acid per peptide. We found that RMI1 interacted strongly with 12 consecutive peptides, all containing the region corresponding to $BLM_{35–40}$ (Fig. 5C).

To define precisely which amino acids are essential within this region, we generated a mutant peptide array of 20-mer peptides containing the conserved region of BLM important for RMI1 interaction. In this array, the 20 amino acids corresponding to $BLM_{27–46}$ were sequentially substituted to leucine, glycine, arginine, or glutamate. When this membrane was probed for RMI1 interaction, we observed that substitution of Phe35 with another amino acid abolished interaction. Similarly, substitution of Thr36 or Phe37 led to a loss of interaction with RMI1 (Fig. 5D). All three amino acids, along with the adjacent lysine residues, are invariant across vertebrate evolution.

We demonstrated the critical nature of the $^{35}FTF^{37}$ sequence for RMI1 association using pull-down and fluorescence anisotropy
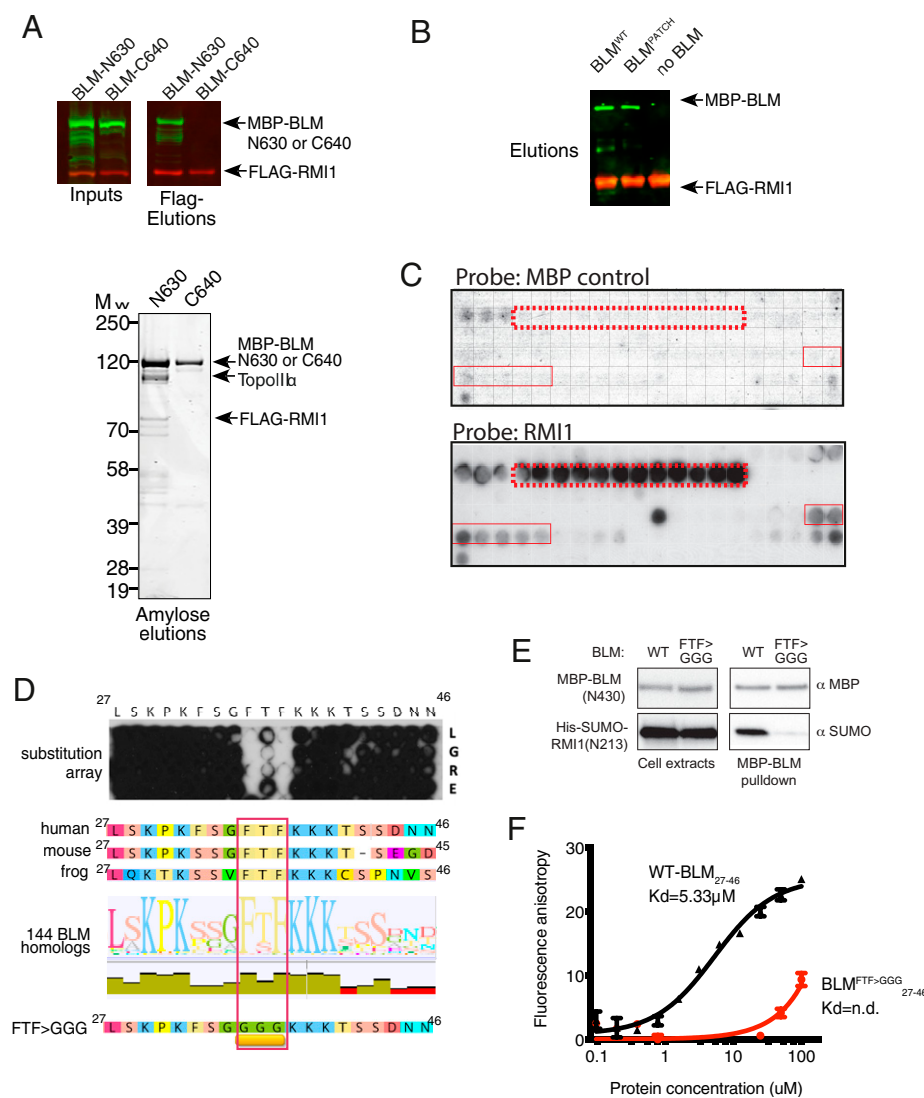
Fig. 5. A conserved N-terminal motif in BLM mediates TopoIIIα:RMI1:RMI2 association independent of BLM dimerization. (A and B) Elutions from coimmunoprecipitation of the Flag-RMI1:RMI2:TopoIIIα complex with BLM N630 or C640 of full-length BLM[WT] or BLM[PATCH]. (C) Overlapping peptide array of $BLM_{1–120}$. Spot 1 = $BLM_{1–20}$, spot 2 = $BLM_{2–21}$, etc. incubated with MBP (*Upper*) or HisSUMO-$RMI1_{1–213}$ (*Lower*) and then probed with anti-MBP antibody. (D) Substitution peptide array. Each amino acid (columns) of $BLM_{27–46}$ is substituted with (row 1) leucine, (row 2) glycine, (row 3) arginine, or (row 4) glutamate. Beneath the array is an alignment of $BLM_{27–46}$ from human, mouse (*Mus musculus*), or frog (*Xenopus laevis*) plus motif logo from 144 vertebrate homologs. The conserved FTF sequence is highlighted, and the mutant used in the experiments is indicated. (E) Pulldown experiment with recombinant BLM and wild-type (WT) or mutant (FTF>GGG) RMI1 fragments. (F) Example fluorescence polarization experiments performed using $BLM_{27–46}$ or $BLM_{27–46}^{FTF > GGG}$ and $RMI1_{1–213}$.

Hodson et al.
Mechanism of Bloom syndrome complex assembly required for double Holliday junction dissolution and genome stability

PNAS | 7 of 12
https://doi.org/10.1073/pnas.2109093119

experiments. We used an N-terminal fragment of RMI1 (residues 1 to 213), which can be purified in the absence of RMI2 and Top-oIIIα (19). This fragment bound wild-type BLM N433 but not BLM N433$^{FTF > GGG}$ (Fig. 5E and *SI Appendix*, Fig. S3B). By fluorescence anisotropy, a clear interaction was observed between the wild-type BLM$_{27–40}$ and RMI1-N213 fragments, with a dissociation constant of 5 μM. When BLM$_{27–40}$$^{FTF > GGG}$ peptide was used, it was not possible to determine a dissociation constant at a maximum protein concentration of 100 μM, confirming that the association is drastically weakened (Fig. 5F).

Our XL-MS data also show multiple cross-links between BLM and the C-terminal zinc finger domains of TopoIIIα (Fig. 2D). These interactions were confirmed in pull-down experiments using Flag-tagged fragments of TopoIIIα expressed in human cells; a fragment containing the four zinc fingers can strongly coimmunoprecipitate BLM but not RMI1 (*SI Appendix*, Fig. S4). However, despite several attempts, we were never able to generate a suitable fragment of the TopoIIIα protein to perform interaction experiments similar to those conducted for RMI1. The critical residues required for interaction of BLM with TopoIIIα have, therefore, not yet been determined.

Inhibition of Dimerization or BS Assembly Prevents the dHJ Dissolution Activity of the BS Complex.

Given that dimerized BLM is the predominant form of the protein within a stable recombinant BS complex, we next asked whether dimerization is important for the ability of the complex to dissolve dHJs. We first purified BLM^{WT} or BLM^{PATCH} proteins. These proteins showed comparable activity in real-time helicase assays that measure ATP-dependent unwinding of branched fluorescently labeled DNA molecules (Fig. 6A), suggesting that BLM homodimerization is unnecessary for either the ATPase or the DNA unwinding activities of the protein.

However, when we compared the activities of BLM^{WT} to BLM^{PATCH} (or the RMI1 binding defective mutant BLM$^{FTF > GGG}$) using in vitro dHJ dissolution assays together with the TopoIIIα-RMI1-RMI2 complex, we found that both mutant complexes displayed remarkably reduced activity only slightly above the negligible levels seen with an ATPase-defective BLM^{K695T} (Fig. 6B). Time course experiments indicated that the initial rate of BS^{PATCH} complex activity is at least sevenfold lower than for the wild-type BS complex (Fig. 6C).

Given that the BS^{PATCH} complex contains only one copy of each component of the BS complex, we next determined if a dimeric BS complex containing only one active helicase is functional. We, therefore, used tandem affinity purification to isolate a BLM heterodimer containing one subunit of truncated MBP-BLM (N630, no helicase but dimer and TopoIIIα binding competent) and one full-length Flag-BLM (as per Fig. 5A). When mixed with TopoIIIα:RMI1:RMI2, this hybrid dimer of BLM generated five times fewer dissolution products than a similar dimer composed of two full-length entities (Fig. 6D). Together, these data reveal the critical contributions of the dimerization of BLM and its direct coupling to TopoIIIα:RMI1:RMI2 to the dHJ dissolution reaction.

Dimerization of BLM and BLM:TRR Association Is Essential for Genome Stability in Cells.

Our results define the contribution of dimerization and TRR association to the functions of BS complex to aspects of HR reconstituted in vitro. To test whether they are necessary for maintenance of genome stability in cells, we knocked out BLM in human RPE-1 cells as described previously (46). These cells contain a CRISPR-mediated deletion in exon 4 and display no detectable BLM protein by western blot (Fig. 7A). We then generated lines complemented with GFP-BLM^{WT}, -BLM^{PATCH}, -BLM$^{FTF > GGG}$, or -BLM^{K695R} or GFP (green fluorescent protein) alone. Using GFP trap, we found that the FTF > GGG mutation abrogates coimmunoprecipitation of GFP-

BLM with the TopoIIIα-RMI complex but not replication protein A (RPA) (Fig. 7B). Importantly, the BLM^{PATCH} mutant retains normal association with both complexes. These results confirm the findings of our in vitro biochemical experiments.

The RPE-1 BLM$^{−/−}$ cells display an elevation in sister chromad exchange (SCE) levels analogous to that seen in cells from Bloom syndrome patients, and expression of the helicase-dead BLM^{K695R} mutant did not affect this (Fig. 7 C and D).

When complemented with GFP-BLM^{WT}, the level of SCEs is reduced to the level of the parental RPE-1 cell line (Fig. 7 C and D). In contrast, expression of GFP-BLM^{PATCH} or GFP-BLM$^{FTF > GGG}$ failed to fully complement SCE levels, which remain significantly higher than in both the parental and GFP-BLM^{WT} complemented cell lines.

SCE formation in BLM-deficient cells is dependent upon the nuclease activities of SLX4-MUS81 and GEN1 (3). In particular, MUS81 and GEN1 nuclease activities are essential for viability in BLM-deficient cells. As this is hypothesized to be a dHJ-specific phenotype (3, 47), we tested the ability of different variants of BLM to rescue the synthetic growth defect of GEN1/MUS81 codepletion. Combined GEN1/MUS81 small interfering RNA (siRNA) depletion (*SI Appendix*, Fig. S5) caused a >95% reduction in cell viability of BLM-deficient RPE-1 (Fig. 7E). This is in line with previously published results (47, 48). GFP-BLM^{WT} could fully complement this viability deficiency; however, for GFP-BLM^{PATCH}, GFP-BLM$^{FTF > GGG}$, and GFP-BLM^{K695R}, the rescue was incomplete.

When the chromosome spreads from these cells were analyzed at 48 h after GEN1/MUS81 knockdown, we observed accumulation of segmented chromosomes in BLM$^{−/−}$ cells (Fig. 7F). These are a hallmark of cells deficient in dHJ dissolution/resolution and are hypothesized to represent regions of uncondensed chromatin associated with unresolved HR intermediates (3). Because neither GFP-BLM^{PATCH} nor GFP-BLM$^{FTF > GGG}$ mutants could rescue the appearance of these segmented chromosomes when the backup dHJ resolution pathway was inactivated, we conclude that both BLM dimerization and BLM:RMI association are essential for dHJ dissolution and maintenance of genome instability in vivo (Fig. 7F).

Discussion

BLM functions in several critical steps of HR, including in controlling the extent of resection, the displacement of heterologous invasion intermediates created by RAD51, and the final step of dHJ dissolution. This places the protein at the heart of decision making relating to the fidelity of HR outcomes, an essential process in tumor avoidance (11). Whereas the Top-oIIIα catalytic activity and RMI1:RMI2 components of the BS complex are critical to BLM's role in dHJ dissolution, they also stimulate both resection and D-loop displacement. Interestingly, a catalytically dead version of TopoIIIα can still stimulate the in vitro activity of BLM homolog SGS1 in resection (49). In the equivalent yeast complex, the decatenation activity of Top-oIIIα is also stimulated by an inactive Sgs1 (BLM homolog) (10). Coimmunoprecipitation experiments confirm that BLM and TopoIIIα are rarely found in an uncomplexed state (50). These findings indicate that BLM probably participates within the BS complex for most or all of its in vivo functions, even though it does not always require the catalytic activity of Top-oIIIα. The findings reported here indicate that the BS complex is a stable complex through several steps of purification.

How Does the BS Complex Assembly Mediate dHJ Dissolution?

An important unanswered question regarding BS complex activity relates to how the helicase and topoisomerase domains within the BS complex are coordinated for dHJ dissolution. One hypothesis is derived by analogy with studies on the
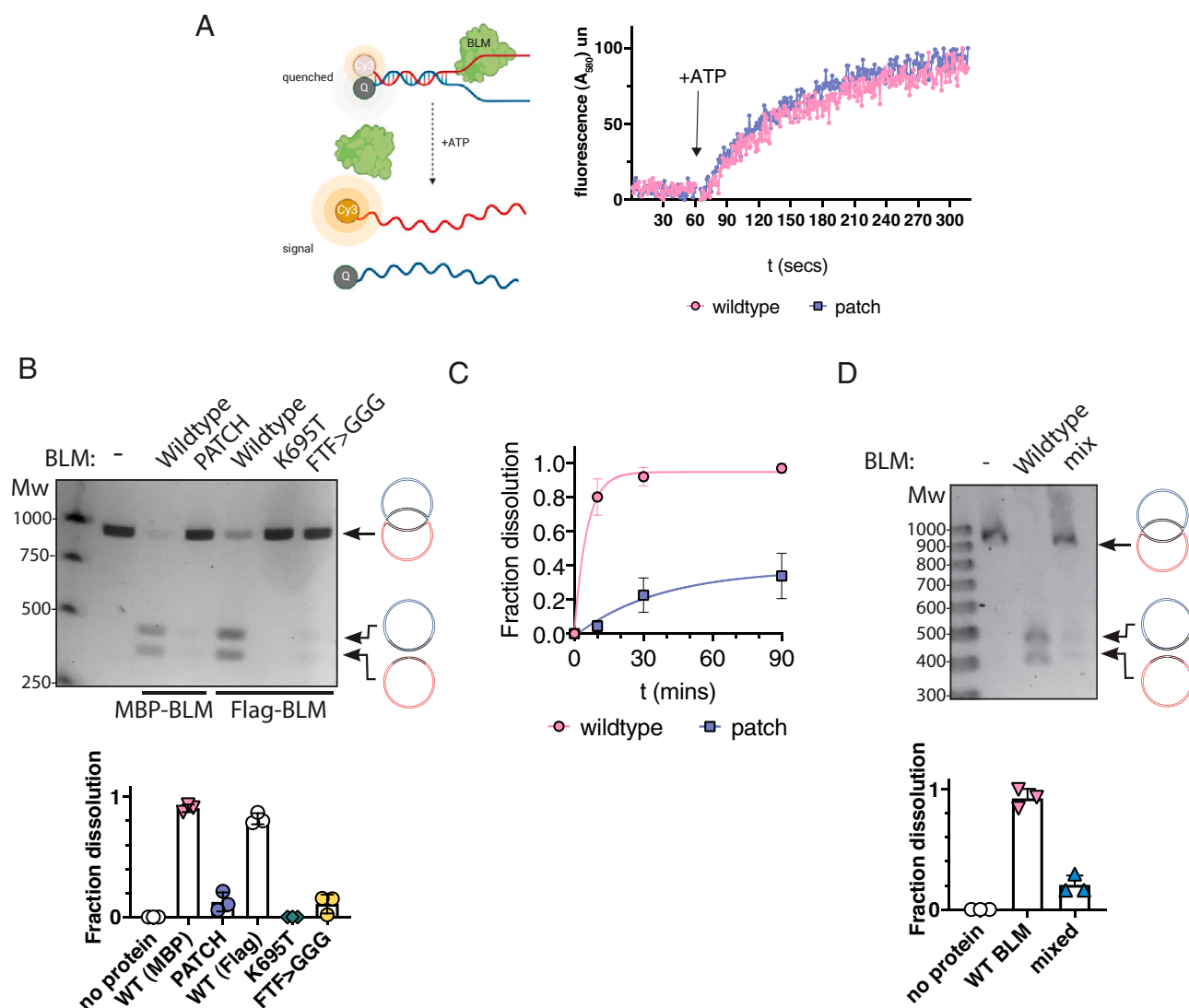
Fig. 6. BLM dimerization is required for dHJ dissolution but not helicase activity of BS complex. (*A*) Real-time helicase assays of wild-type and PATCH (dimerization-defective mutant) BLM proteins. ATP was injected at the indicated time point. (*B*) Example dHJ assay result (30 min) of the dissolution assay with wild-type, PATCH, FTF > GGG, or K695T BLM proteins together with the TopoIIIα:RMI1:RMI2 complex. (*C*) Time course experiment showing progress of dissolution from an average of three experiments with MBP-BLM or MBP-BLM-PATCH together with the TopoIIIα::RMI1:RMI2 complex. (*D*) Example dHJ assay (30 min) using Flag-BLM in complex with MBP-BLM wild type or MBP-BLM-N630 together with the TopoIIIα::RMI1:RMI2 complex. Graphs of three independent experiments ± SEM are shown beneath each example in *B* and *D*. WT, wild type.

homologous bacterial system, where RecQ and TopoIII cooperate to segregate late replication intermediates by acting on an interlinked DNA substrate (similar to a dHJ) (51). In this "unravel and unlink" model, BLM and TopoIIIα do not necessarily need to interact. Instead, BLM could unwind large heteroduplex regions, leaving the uncoupled action of TopoIIIα to dissipate topological linkages and eventually decatenate a focused dHJ (hemicatenane) during the final step of DNA cross-over dissolution (52). According to an alternative model, named "HJ migration," BLM and TopoIIIα could coordinate their activity to promote branch migration. Here, BLM would push an HJ forward while driving the comigration of TopoIIIα, poised to perform coordinated strand passage on each heteroduplex (40, 51). In our hands, the overall stability of the BS complex through several protein purification steps directly supports the stability of a complex that requires direct coupling. We infer that coordinated ATPase/topoisomerase activity must occur at some point during the dissolution reaction.

To allow for strand passage within the context of an HJ, it has been proposed that an extended period of opening, between domains 1 and 3 of TopoIIIα, would be required for intermolecular strand passage. Our cross-linking experiments point to a critical engagement of the N terminus of BLM with domain 3/4 and the zinc finger motifs of TopoIIIα. We propose that the strong ssDNA binding preferences of each of these three regions (40, 53, 54) intersect to stabilize intermediates created by the helicase domain of BLM. In this manner, gate opening time is extended to allow for "intermolecular" strand passage during HJ migration. Close structural investigation of the mechanism by which the N terminus of BLM intersects with the C-terminal half of TopoIIIα will be critical to further understand this process.

An Important Role for Dimerization within the BS Complex. Our data indicate that within the BS complex, there are two copies of BLM helicase, like what was observed by atomic force
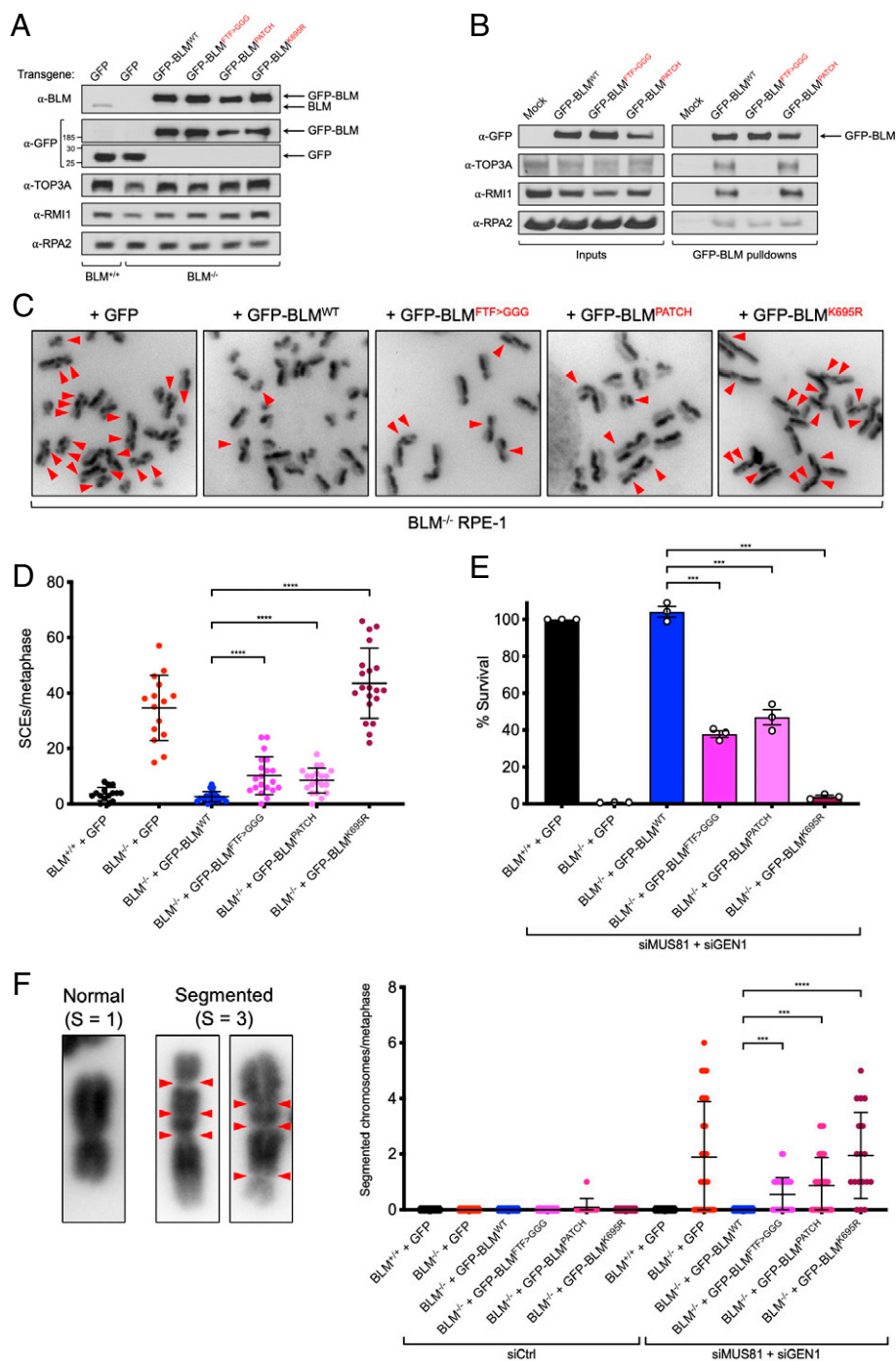
Fig. 7. BLM dimerization and RMI1 association are required for genome stability in cells. (*A*) Western blots of BLM^{+/+} and BLM^{−/−} RPE-1 cells complemented with GFP or GFP-BLM variants. (*B*) Coimmunoprecipitations from cells transfected with GFP-BLM variants. (*C*) Representative mitotic chromosomes and (*D*) quantification of SCEs/mitosis. Error bars indicate SD. (*E*) Colony survival assays with BLM^{+/+} and BLM^{−/−} RPE-1 cells complemented with GFP or GFP-BLM variants and transfected with control or MUS81/GEN1 siRNAs. Error bars indicate SEM. (*F*) Examples of normal and segmented chromosomes from the cells treated as in *E* and their quantification. Error bars indicate SD. ***$P < 0.001$, ****$P < 0.0001$.

microscopy (25). However, other studies have suggested a hexameric or higher-oligomer state. In particular, negative stain EM imaging of the recombinant BLM protein revealed structures that appear hexameric (24). We note that these particles match short-angle views of a BLM dimer in which electron density features would correspond to the RecA1, RecA2, and RQC/HRDC domain of BLM, arranged in exactly the configuration predicted by our chemical cross-linking and molecular modeling data (*SI Appendix*, Fig. S2). Like others (24), we also observed BLM running considerably higher in SEC than the predicted size of a dimer. However, SEC sizing is only accurate when the proteins being measured are spherical (55), whereas SEC-MALS gives an absolute measure of molecular mass,

which in our case, indicates a dimer structure of the BLM N terminus in solution. The absence of detectable intraprotein cross-links from the N terminus of BLM suggests that it is probably in a very extended conformation, which was also predicted by others (56).

Several key questions concerning dHJ dissolution are raised by the discovery of the dimeric BS complex. First, how is the polarity of substrate engagement controlled to ensure that dHJs are migrated convergently? Perhaps the involvement of BLM in the early resection step of recombination leads to loading of the BS complex in the correct orientation for subsequent convergent migration after synapsis. An early report indicates that BS complex remains associated with D loops in an in vitro

reaction containing BLM and other elements required for resection and synapsis, including RAD51, Exo1, and RPA (57). However, that study did not observe the subsequent steps of second end capture, extension, and ligation required to test whether dHJ would then be activated by the HJ-associated BS complex. A second open question is whether both HJ are engaged by distinct BS complexes. With a single dimeric BS complex and a topoisomerase removing supercoiling on each converging DNA molecule, it may be sufficient for a single BS complex to directionally migrate only one HJ, while the other remains static. Stasis could be maintained passively or by the action of another HJ binding protein or ongoing D-loop extension by a polymerase. Third, how do other interaction partners influence, or arise from, the BLM dimerization state? In particular, RPA is a critical regulator of dHJ dissolution by the BS complex, and two RPA binding motifs have been identified on either side of the DHBN domain (46, 58). We show that dimerization and RMI binding mutants of BLM retain normal coimmunoprecipitation of RPA, but future work should explore the effect of dimerization on RPA engagement and dHJ processing. Fourth, how do protein modification events regulate the activity of the BS complex? Various kinases and ubiquitin or SUMO ligases have been shown to regulate the activity of BLM but not in the context of BS complex assembly. As the N terminus of BLM is most heavily regulated by these enzymes, such modifications could positively or negatively regulate dynamic assembly of dimers or RMI1/TopoIIIα interaction. This would have different consequences at different stages of HR, and reconstitution of the entire HR process would be required to further test these theories.

Potential Implications for Heterozygous Carriers of BLM Mutations.

N-terminal dimerization of BLM suggests that a dominant-negative mode of action may occur in heterozygous carriers of truncating mutations in BLM. If a truncated protein was stably produced from such alleles, it would likely form dimers with the wild-type product. Based on our studies and others, N-terminal fragments could also bind RMI1 and TopoIIIα (11, 59). Although other molecular mechanisms may also be involved, our results suggest that truncated mutants would act in a classical dominant interfering capacity and reduce the functional BS complexes on dHJ dissolution in cells by greater than the 50% reduction in functional wild-type BLM protein. In one study where this has been investigated, elevated sister chromatid exchanges were observed in a family carrying the c.3617–3619delAA (p.K1207fsX9) variant (60). Other evidence comes from two different Blm mutant mouse models, one of which retains a truncated gene, while the other is a complete null (61, 62). In both cases, homozygous mutant mice displayed increased SCEs, which associate with loss of heterozygosity at tumor suppressor loci, and malignancy. However, in heterozygotes, a phenotype of increased SCEs is only observed in the mouse that can express truncated (i.e., dominant) BLM protein (62).

In women, BLM-truncating variants were statistically overrepresented in 2,000 non-BRCA1/2 breast cancer families and were shown to cosegregate with disease where three or more generations of individuals could be genetically tested (6). A different BLM truncation, which is carried by more than 1% of the Ashkenazi population, does not seem to predispose to breast or other cancers (63). It is possible that some mutations produce a dominant-negative peptide, while others do not.

Further studies to identify expression levels of various truncated BLM variants would be useful to test this hypothesis.

Conclusions. The studies presented here provide structural information about overall BS complex assembly and dimerization. The high fidelity of HR requires the regulatory activity of the BS complex, which can otherwise create repeat deletions, chromosomal translocations, loss of heterozygosity, and other protumorigenic DNA changes. Recent studies have also pointed to critical roles for the BS complex in meiosis (64), innate immunity (65), gene editing (66), and chemotherapy response (67). The key findings of our work, including mutants, could be key to identifying a role of dimerization and direct BLM:RMI1 interaction in each of these essential BS complex–dependent processes.

Materials and Methods

Detailed methods are provided in *SI Appendix*.

Protein Purification and Analysis. The BTRR complex and derivatives were cloned into recombinant Bacmids using the Multibac system (28). Baculoviruses coexpressing BLM-8HIS, MBP-RMI1, TopoIIIα, and RMI2 were used to infect High Five cells (Invitrogen) at muliplicity of infection (MOI) = 2.5. Proteins were isolated from cells after 3-d expression using amylose and nickel affinity chromatography followed by size exclusion. Other proteins were produced in the *Escherichia coli* BL21 strain. Patch mutant is encoded by a sequence that alters the following underlined residues to alanines: KLIDTIPDDKLKLLDCGNELLQQR-NIRRKLLT. Peptides and peptide arrays were generated in house.

XL-MS. The purified samples were then prepared for XL-MS essentially as described previously (68) using the H_{12}/D_{12}-DSS cross-linker. This final list of verified cross-links can be found in Dataset S1. All raw mass spectrometry data (including spectra) and search results have been deposited in the ProteomeXchange Consortium via the PRIDE partner repository (69) under accession number PXD011078.

Biochemical Assays. The ideal dHJ was generated from four ssDNA circles as previously described (31). Fluorescence resonance energy transfer (FRET)-based DNA unwinding assays were performed as in ref. 70. SEC and SEC-MALS were performed as described in ref. 42.

Cell Lines. RPE-1 $BLM^{-/-}$ cells transduced by lentivirus to express GFP or GFP-BLM were generated and analyzed as in ref. 46 and with MUS81/GEN1 siRNAs (3).

Data Availability. Mass spectrometry data have been deposited in ProteomeXchange Consortium via the PRIDE partner repository (accession no. PXD011078). All other data are included in the manuscript and/or supporting information.

1. J. Matos, M. G. Blanco, S. Maslen, J. M. Skehel, S. C. West, Regulatory control of the resolution of DNA recombination intermediates during meiosis and mitosis. *Cell* **147**, 158–172 (2011).
2. K. Zakharyevich, S. Tang, Y. Ma, N. Hunter, Delineation of joint molecule resolution pathways in meiosis identifies a crossover-specific resolvase. *Cell* **149**, 334–347 (2012).
3. T. Wechsler, S. Newman, S. C. West, Aberrant chromosome morphology in human cells defective for Holliday junction resolution. *Nature* **471**, 642–646 (2011).
4. Y. W. Chan, K. Fugger, S. C. West, Unresolved recombination intermediates lead to ultra-fine anaphase bridges, chromosome breaks and aberrations. *Nat. Cell Biol.* **20**, 92–103 (2018).
5. J. German, Bloom's syndrome. XX. The first 100 cancers. *Cancer Genet. Cytogenet.* **93**, 100–106 (1997).
6. E. R. Thompson *et al.*, kConFab, Exome sequencing identifies rare deleterious mutations in DNA repair genes FANCC and BLM as potential breast cancer susceptibility alleles. *PLoS Genet.* **8**, e1002894 (2012).

Hodson et al.
Mechanism of Bloom syndrome complex assembly required for double Holliday junction dissolution and genome stability

PNAS | **11 of 12**
https://doi.org/10.1073/pnas.2109093119

7. D. Prokofyeva *et al.*, Nonsense mutation p.Q548X in BLM, the gene mutated in Bloom's syndrome, is associated with breast cancer in Slavic populations. *Breast Cancer Res. Treat.* **137**, 533–539 (2013).

8. L. Wu, I. D. Hickson, The Bloom's syndrome helicase suppresses crossing over during homologous recombination. *Nature* **426**, 870–874 (2003).

9. J. K. Karow, R. K. Chakraverty, I. D. Hickson, The Bloom's syndrome gene product is a 3′-5′ DNA helicase. *J. Biol. Chem.* **272**, 30611–30614 (1997).

10. P. Cejka, J. L. Plank, C. C. Dombrowski, S. C. Kowalczykowski, Decatenation of DNA by the S. cerevisiae Sgs1-Top3-Rmi1 and RPA complex: A mechanism for disentangling chromosomes. *Mol. Cell* **47**, 886–896 (2012).

11. R. Bythell-Douglas, A. J. Deans, A structural guide to the Bloom syndrome complex. *Structure* **29**, 99–113 (2020).

12. N. Bocquet *et al.*, Structural and mechanistic insight into Holliday-junction dissolution by topoisomerase IIIα and RMI1. *Nat. Struct. Mol. Biol.* **21**, 261–268 (2014).

13. C. F. Chen, S. J. Brill, Binding and activation of DNA topoisomerase III by the Rmi1 subunit. *J. Biol. Chem.* **282**, 28971–28979 (2007).

14. J. R. Mullen, F. S. Nallaseth, Y. Q. Lan, C. E. Slagle, S. J. Brill, Yeast Rmi1/Nce4 controls genome stability as a subunit of the Sgs1-Top3 complex. *Mol. Cell. Biol.* **25**, 4476–4487 (2005).

15. S. Raynard *et al.*, Functional role of BLAP75 in BLM-topoisomerase IIIalpha-dependent holliday junction processing. *J. Biol. Chem.* **283**, 15701–15708 (2008).

16. D. Xu *et al.*, RMI, a new OB-fold complex essential for Bloom syndrome protein to maintain genome stability. *Genes Dev.* **22**, 2843–2855 (2008).

17. A. J. Deans, S. C. West, FANCM connects the genome instability disorders Bloom's Syndrome and Fanconi Anemia. *Mol. Cell* **36**, 943–953 (2009).

18. T. R. Singh *et al.*, BLAP18/RMI2, a novel OB-fold-containing protein, is an essential component of the Bloom helicase-double Holliday junction dissolvasome. *Genes Dev.* **22**, 2856–2868 (2008).

19. F. Wang *et al.*, Crystal structures of RMI1 and RMI2, two OB-fold regulatory subunits of the BLM complex. *Structure* **18**, 1159–1170 (2010).

20. D. F. Hudson *et al.*, Loss of RMI2 increases genome instability and causes a bloom-like syndrome. *PLoS Genet.* **12**, e1006483 (2016).

21. C. A. Martin *et al.*, GOSgene, Mutations in TOP3A cause a bloom syndrome-like disorder. *Am. J. Hum. Genet.* **103**, 221–231 (2018).

22. J. A. Newman *et al.*, Crystal structure of the Bloom's syndrome helicase indicates a role for the HRDC domain in conformational changes. *Nucleic Acids Res.* **43**, 5221–5235 (2015).

23. M. K. Swan *et al.*, Structure of human Bloom's syndrome helicase in complex with ADP and duplex DNA. *Acta Crystallogr. D Biol. Crystallogr.* **70**, 1465–1475 (2014).

24. J. K. Karow, R. H. Newman, P. S. Freemont, I. D. Hickson, Oligomeric ring structure of the Bloom's syndrome helicase. *Curr. Biol.* **9**, 597–600 (1999).

25. M. Gyimesi *et al.*, Visualization of human Bloom's syndrome helicase molecules bound to homologous recombination intermediates. *FASEB J.* **27**, 4954–4964 (2013).

26. C. F. Chen, S. J. Brill, Multimerization domains are associated with apparent strand exchange activity in BLM and WRN DNA helicases. *DNA Repair (Amst.)* **22**, 137–146 (2014).

27. S. F. Beresten *et al.*, Purification of overexpressed hexahistidine-tagged BLM N431 as oligomeric complexes. *Protein Expr. Purif.* **17**, 239–248 (1999).

28. I. Berger, D. J. Fitzgerald, T. J. Richmond, Baculovirus expression system for heterologous multiprotein complexes. *Nat. Biotechnol.* **22**, 1583–1587 (2004).

29. H. Goulaouic *et al.*, Purification and characterization of human DNA topoisomerase IIIalpha. *Nucleic Acids Res.* **27**, 2443–2450 (1999).

30. J. K. Karow, A. Constantinou, J. L. Li, S. C. West, I. D. Hickson, The Bloom's syndrome gene product promotes branch migration of holliday junctions. *Proc. Natl. Acad. Sci. U.S.A.* **97**, 6504–6508 (2000).

31. J. L. Plank, T.-S. Hsieh, A novel, topologically constrained DNA molecule containing a double Holliday junction: Design, synthesis, and initial biochemical characterization. *J. Biol. Chem.* **281**, 17510–17516 (2006).

32. A. Leitner *et al.*, Expanding the chemical cross-linking toolbox by the use of multiple proteases and enrichment by size exclusion chromatography. *Mol. Cell Proteomics* **11**, M111.014126 (2012).

33. O. Rinner *et al.*, Identification of cross-linked peptides from large sequence databases. *Nat. Methods* **5**, 315–318 (2008).

34. B. Yang *et al.*, Identification of cross-linked peptides from complex samples. *Nat. Methods* **9**, 904–906 (2012).

35. Z. A. Chen *et al.*, Architecture of the RNA polymerase II-TFIIF complex revealed by cross-linking and mass spectrometry. *EMBO J.* **29**, 717–726 (2010).

36. A. Kahraman, L. Malmström, R. Aebersold, Xwalk: Computing and visualizing distances in cross-linking experiments. *Bioinformatics* **27**, 2163–2164 (2011).

37. A. Leitner *et al.*, Chemical cross-linking/mass spectrometry targeting acidic residues in proteins and protein complexes. *Proc. Natl. Acad. Sci. U.S.A.* **111**, 9455–9460 (2014).

38. M. Mills, Y.-C. Tse-Dinh, K. C. Neuman, Direct observation of topoisomerase IA gate dynamics. *Nat. Struct. Mol. Biol.* **25**, 1111–1118 (2018).

39. X. Duan, J. A. Hall, H. Nikaido, F. A. Quiocho, Crystal structures of the maltodextrin/maltose-binding protein complexed with reduced oligosaccharides: Flexibility of tertiary structure and ligand binding. *J. Mol. Biol.* **306**, 1115–1126 (2001).

40. S. H. Chen, C. H. Wu, J. L. Plank, T. S. Hsieh, Essential functions of C terminus of Drosophila Topoisomerase IIIα in double Holliday junction dissolution. *J. Biol. Chem.* **287**, 19346–19353 (2012).

41. L. Wu *et al.*, The Bloom's syndrome gene product interacts with topoisomerase III. *J. Biol. Chem.* **275**, 9636–9644 (2000).

42. P. Swuec *et al.*, The FA core complex contains a homo-dimeric catalytic module for the symmetric mono-ubiquitination of FANCI-FANCD2. *Cell Rep.* **18**, 611–623 (2017).

43. P. Alcón *et al.*, FANCD2-FANCI is a clamp stabilized on DNA by monoubiquitination of FANCD2 during DNA repair. *Nat. Struct. Mol. Biol.* **27**, 240–248 (2020).

44. A. C. Pike *et al.*, Human RECQ1 helicase-driven DNA unwinding, annealing, and branch migration: Insights from DNA complex structures. *Proc. Natl. Acad. Sci. U.S.A.* **112**, 4286–4291 (2015).

45. J. Shi *et al.*, A helical bundle in the N-terminal domain of the BLM helicase mediates dimer and potentially hexamer formation. *J. Biol. Chem.* **292**, 5909–5920 (2017).

46. A. K. Shorrocks *et al.*, The Bloom syndrome complex senses RPA-coated single-stranded DNA to restart stalled replication forks. *Nat. Commun.* **12**, 585 (2021).

47. E. Garner, Y. Kim, F. P. Lach, M. C. Kottemann, A. Smogorzewska, Human GEN1 and the SLX4-associated nucleases MUS81 and SLX1 are essential for the resolution of replication-induced Holliday junctions. *Cell Rep.* **5**, 207–215 (2013).

48. H. D. Wyatt, S. Sarbajna, J. Matos, S. C. West, Coordinated actions of SLX1-SLX4 and MUS81-EME1 for Holliday junction resolution in human cells. *Mol. Cell* **52**, 234–247 (2013).

49. H. Niu *et al.*, Mechanism of the ATP-dependent DNA end-resection machinery from *Saccharomyces cerevisiae*. *Nature* **467**, 108–111 (2010).

50. A. R. Meetei *et al.*, A multiprotein nuclear complex connects Fanconi anemia and Bloom syndrome. *Mol. Cell. Biol.* **23**, 3417–3426 (2003).

51. J. Plank, T. S. Hsieh, Helicase-appended topoisomerases: New insight into the mechanism of directional strand transfer. *J. Biol. Chem.* **284**, 30737–30741 (2009).

52. C. Suski, K. J. Marians, Resolution of converging replication forks by RecQ and topoisomerase III. *Mol. Cell* **30**, 779–789 (2008).

53. C. F. Cheok, L. Wu, P. L. Garcia, P. Janscak, I. D. Hickson, The Bloom's syndrome helicase promotes the annealing of complementary single-stranded DNA. *Nucleic Acids Res.* **33**, 3932–3941 (2005).

54. K. Perry, A. Mondragón, Structure of a complex between *E. coli* DNA topoisomerase I and single-stranded DNA. *Structure* **11**, 1349–1358 (2003).

55. J. Wen, T. Arakawa, J. S. Philo, Size-exclusion chromatography with on-line light-scattering, absorbance, and refractive index detectors for studying proteins and their interactions. *Anal. Biochem.* **240**, 155–166 (1996).

56. J. A. Kennedy, G. W. Daughdrill, K. H. Schmidt, A transient α-helical molecular recognition element in the disordered N-terminus of the Sgs1 helicase is critical for chromosome stability and binding of Top3/Rmi1. *Nucleic Acids Res.* **41**, 10215–10227 (2013).

57. A. V. Nimonkar, A. Z. Ozsoy, J. Genschel, P. Modrich, S. C. Kowalczykowski, Human exonuclease 1 and BLM helicase interact to resect DNA and initiate DNA repair. *Proc. Natl. Acad. Sci. U.S.A.* **105**, 16906–16911 (2008).

58. K. M. Doherty *et al.*, Physical and functional mapping of the replication protein A interaction domain of the Werner and Bloom syndrome helicases. *J. Biol. Chem.* **280**, 29494–29505 (2005).

59. P. Hu *et al.*, Evidence for BLM and Topoisomerase IIIalpha interaction in genomic stability. *Hum. Mol. Genet.* **10**, 1287–1298 (2001).

60. G. Ben Salah *et al.*, A novel frameshift mutation in BLM gene associated with high sister chromatid exchanges (SCE) in heterozygous family members. *Mol. Biol. Rep.* **41**, 7373–7380 (2014).

61. N. van Wietmarschen *et al.*, BLM helicase suppresses recombination at G-quadruplex motifs in transcribed genes. *Nat. Commun.* **9**, 271 (2018).

62. G. Luo *et al.*, Cancer predisposition caused by elevated mitotic recombination in Bloom mice. *Nat. Genet.* **26**, 424–429 (2000).

63. H. N. Baris *et al.*, Prevalence of breast and colorectal cancer in Ashkenazi Jewish carriers of Fanconi anemia and Bloom syndrome. *Isr. Med. Assoc. J.* **9**, 847–850 (2007).

64. J. K. Holloway, M. A. Morelli, P. L. Borst, P. E. Cohen, Mammalian BLM helicase is critical for integrating multiple pathways of meiotic recombination. *J. Cell Biol.* **188**, 779–789 (2010).

65. M. Gratia *et al.*, Bloom syndrome protein restrains innate immune sensing of micronuclei by cGAS. *J. Exp. Med.* **216**, 1199–1213 (2019).

66. C. D. Richardson *et al.*, CRISPR-Cas9 genome editing in human cells occurs via the Fanconi anemia pathway. *Nat. Genet.* **50**, 1132–1139 (2018).

67. C. Cunniff, J. A. Bassetti, N. A. Ellis, Bloom's syndrome: Clinical spectrum, molecular pathogenesis, and cancer predisposition. *Mol. Syndromol.* **8**, 4–23 (2017).

68. J. W. Schmidberger *et al.*, The MTA1 subunit of the nucleosome remodeling and deacetylase complex can recruit two copies of RBBP4/7. *Protein Sci.* **25**, 1472–1482 (2016).

69. J. A. Vizcaíno *et al.*, The PRoteomics IDEntifications (PRIDE) database and associated tools: Status in 2013. *Nucleic Acids Res.* **41**, D1063–D1069 (2013).

70. W. Castillo-Tandazo *et al.*, ATP-dependent helicase activity is dispensable for the physiological functions of Recql4. *PLoS Genet.* **15**, e1008266 (2019).